

HyperScience International Journal

Original Research Papers Open Access Journals

ISSN: 2821-3300

HIJ, Vol 4, No 4, pp 58-71, Dec 2024 https://doi.org/10.55672/hij2024pp58-71 J.R.Farmer

Solar Flares and the Aether Dynamic

Muhammad Aslam Musakhail



Independent Researcher, Main Saddar bazar Musakhail, Pakistan aslammusakhail@gmail.com

James Russell Farmer *



Independent Researcher, 10 William Ave, Greenlane, Auckland 1051, New Zealand jrfarmer12@yahoo.com.au

ABSTRACT

This study investigates the dynamics of Solar flares using the "closed fluid dynamic principle" proposed by Muhammad Aslam Musakhail, which reinforces the pre-Einsteinian aether theory. By defining the "aether force" as the difference between relativistic total mass and rest mass, the principle provides a novel perspective on the relativistic transitions in Solar flare phenomena. The analysis builds on Parker's force-free model and Melrose's resistive slab theory, extending them to describe the dual-phase dynamics of Solar flares: the Alfvénic phase, where massive fermions (v<c) propagate as Alfvén waves, and the heat-dissipation phase, where fermions transition to massless states (v=c), driven by current sources. Key results reveal that energy dissipation scales with resistivity, and the temporal evolution of Poynting flux and magnetic fields highlights distinct transitions between the phases. Numerical simulations demonstrate the exponential decay of axial magnetic fields and the helical organization of flux tubes. These findings validate theoretical predictions and provide insights into particle acceleration, magnetic reconnection, and energy transfer mechanisms during Solar flares. This work not only advances the understanding of Solar flare energetics but also establishes a mathematical framework that can be extended to other astrophysical phenomena, such as cosmic ray acceleration and stellar flares. Future studies should focus on numerical validation and observational testing to refine the dual-phase model and its broader applicability.

Keywords: Alfvénic Dynamics, Force-Free Model, Energy Dissipation, Aether Dynamics

©2024 The Authors, Published by Hyperscience International Journal. This is an open-access article under the CC **BY-NC**

https://creativecommons.org/licenses/bv-nc/4.0/

INTRODUCTION

The dynamic processes underlying Solar flares have long been a subject of astrophysical interest due to their complex interplay between electromagnetic forces, particle physics, and relativistic dynamics.

Building upon the foundational models proposed by Parker and Melrose [1, 2], this paper extends the "closed fluid dynamic principle" of Muhammad Aslam Musakhail to rigorously explore the dual-phase nature of Solar flares [3] within the framework of the aether theory. Solar flares, phenomena resulting from the Sun's magnetic reconnection processes, exhibit two distinct but overlapping phases:

Alfvénic Phase

Characterized by massive fermions propagating subluminally (v < c) as Alfvén waves [4], driven by a potential source. This phase corresponds to Parker's "force-free" model [5].

• Heat-Dissipation Phase

Defined by the transition of fermions to massless particles (v = c), behaving as weak-strong gauge bosons, sustained by current sources [6]. The mathematical investigation centers on Parker's $f(\varpi)$ function, where ϖ denotes the radial position within the Solar flare flux tube. This function is critical in describing the flux tube's electromagnetic fields and current densities [7].

By analogy with the "twin paradox" in special relativity, we explore three key values of $f(\varpi)$, $f(\varpi) = 0$, 1/2, 1, drawing connections between the relativistic dynamics of Solar flares and the foundational principles of general relativity [8]. These values reflect critical transitions within the system:

- $f(\varpi) = 0$: No acceleration or flux interaction.
- $f(\varpi) = \frac{1}{2}$: Intermediate dynamical state.
- $f(\varpi) = 1$: Maximum energy dissipation, corresponding to the completion of the heat-Dissipation Phase.

The flux tube dynamics are analyzed using two formulations of the Poynting vector. The outgoing flux **S** is expressed as:

$$S_z' = S_z'(B_z(\varpi), B_{az}(\varpi), f(\varpi))$$
 (1)

where $B_z(\varpi)$ and $B_{az}(\varpi)$ are the axial and azimuthal magnetic field components, respectively. The associated current density is given by:

$$J_z' = J_z'(\varpi, B_{az}(\varpi), f(\varpi))$$
 (2)

These formulations are derived using Parker's force-free model [2, 5], which simplifies the magnetic field as:

$$B_{\rm az}(\varpi)^2 = -\frac{1}{2}\varpi F'(\varpi)$$

$$B_z(\varpi)^2 = F(\varpi) + \frac{1}{2}\varpi F'(\varpi)$$
(3)

Assuming $F(\varpi) = \varpi$ and $F'(\varpi) = 1$, the magnetic field transitions are modeled as:

$$B_{az}(\varpi)^2 = -\frac{1}{2}\varpi$$

$$B_z(\varpi)^2 = \varpi + \frac{1}{2}\varpi$$
(4)

This introduction lays the foundation for a detailed investigation into the dynamic interactions of massive and massless particles within Solar flare flux tubes. By coupling these models with the principles of special and general relativity [8, 9], this study aims to bridge classical astrophysics and modern relativistic physics, providing insights into the energetics and stability of Solar flares.

LITERATURE REVIEW

The study of Solar flares involves the interplay of particle physics, electromagnetic theory, and astrophysical dynamics. The existing literature forms a foundation for the mathematical and physical insights presented in this paper, with particular emphasis on Parker's force-free model [2] and Melrose's contributions to Solar flare flux tube dynamics [3, 10, 11].

This section reviews key studies and theories, highlighting their relevance to the dual-phase Solar flare model. Here the key propositions and theoretical foundations are as:

1. Photon Properties and Duality

The paper adopts a novel view of photons as "massless fermions," such as electrons and positrons (e^-/e^+) stripped of their rest mass, propagating at the speed of light. Two critical properties of photons are asserted [10-12].

• Relativistic Mass

While photons have zero rest mass $(m_0 = 0)$, they possess relativistic mass given by:

$$E^{2} = (pc)^{2} + (m_{0}c^{2})^{2}, m = \frac{m_{0}}{\sqrt{1 - \frac{v^{2}}{c^{2}}}}$$
(5)

• Electric Charge

Photons exhibit electric charge, evident in their helical propagation along the surfaces of electromagnetic flux tubes.

2. Lorentz Force and Photon Behavior

The behavior of photons under the Lorentz force is critical to understanding flux tube dynamics:

$$F = q(E + v \times B) = 0 \Longrightarrow E = -v \times B \tag{6}$$

Using the relationships E/B = c and $P = 1/\mu$ ($E \times B$), photon propagation aligns with the direction of the Poynting vector.

3. Parker's Force-Free Model

Parker's model introduces a function $f(\varpi)$, dependent on the radial position ϖ , to describe the electromagnetic behavior of Solar flare flux tubes [2]. The axial $(B_z(\varpi))$ and azimuthal $(B_{az}(\varpi))$ magnetic fields are formulated as:

$$B_{az}(\varpi)^{2} = -\frac{1}{2}\varpi F'(\varpi)$$

$$B_{z}(\varpi)^{2} = F(\varpi) + \frac{1}{2}\varpi F'(\varpi)$$
(7)

4. Melrose's Contributions

Melrose extended Parker's work by proposing a resistive slab model and a radial electric field for flux tubes [1, 3]. His framework integrates an electromagnetic 4-vector representation:

$$\mathbf{A} = (J \cdot E, E \times B) \tag{8}$$

which this study leverages to elucidate the dual-phase Solar flare model.

Gaps and Contributions

While Parker and Melrose provided significant insights into Solar flare flux tube dynamics, the dual-phase nature of Solar flares and their transition between Alfvénic and Heat-Dissipation Phase remain inadequately addressed. This study builds on their work by:

- Bridging the gap between massive and massless particle dynamics in Solar flares.
- Introducing mathematical models to analyze the interplay between potential and current sources across phases.
- Employing advanced 4-vector formulations to describe electromagnetic flux dynamics comprehensively.

This paper integrates theoretical insights from the works of Parker [2], Melrose [1], and Einstein [10], combining classical models with modern relativistic approaches. By synthesizing these perspectives, the study aims to provide a cohesive understanding of Solar flare energetics, transitioning from force-free to heat-dissipation dynamics.

METHODOLOGY

The methodology employed in this study combines theoretical physics, mathematical modeling, and astrophysical insights to investigate the dynamics of Solar flares through the lens of the "aether dynamic principle." This section outlines the step-by-step framework used to derive and analyze the dual-phase model, integrating principles from Einstein's relativity [9], Parker's force-free model [2], and the novel "ultimate relativity" extension.

1. Aether Dynamics and Relativity Framework

The study builds on the "aether dynamic principle," which introduces the concept of an aether force [13, 14], F(v), defined as the difference between relativistic and rest masses:

$$F(v) = m_{\text{rel}} - m_0 = \frac{m_0}{\sqrt{1 - \frac{v^2}{c^2}}} - m_0$$
(9)

This principle was used to address the "twin paradox" in special relativity. Unlike classical relativity, which neglects acceleration effects, the aether dynamic framework incorporates acceleration phases to resolve the clock discrepancies of the twins.

This necessitates modifying the Newtonian force equation, F = ma to include relativistic corrections under aether dynamics [14, 15].

2. Transitioning from the Twin Paradox to Solar Flare Dynamics

Energy release in solar flares occurs during the impulsive phase [16, 17]. The study bridges the gap between the twin paradox resolution and Solar flare modeling [17, 18]. Solar flares are analyzed [19] as relativistic systems where particles transition between massive (v < c) and massless (v = c) states, analogous to the clock acceleration phase in the twin paradox. This is described mathematically by:

$$E^{2} = (pc)^{2} + (m_{0}c^{2})^{2}$$
 (10)

and by considering the relativistic nature of the propagating fermions:

$$m = \frac{m_0}{\sqrt{1 - \frac{v^2}{c^2}}} \tag{11}$$

3. Dual-Phase Solar Flare Model

Solar flares are modeled as flux tubes undergoing two overlapping phases.

a. Alfvénic Phase (Potential Source)

Governed by Parker's force-free model, where massive fermions propagate as Alfvén waves[4, 20]. The electromagnetic fields are described by:

$$B_{\rm az}(\varpi)^2 = -\frac{1}{2}\varpi F'(\varpi)$$

$$B_z(\varpi)^2 = F(\varpi) + \frac{1}{2}\varpi F'(\varpi)$$
(12)

Here, ϖ is the radial coordinate, and $F(\varpi)$ represents a flux function.

b. Heat-dissipation Phase (Current Source)

Characterized by massless fermions propagating at the velocity v = c. This phase introduces heat dissipation due to interactions of fermions and electromagnetic fields, modeled as:

$$P = I \cdot E \tag{13}$$

where *I* is the current density and *E* the electric field.

4. Mathematical Derivation of Flux Tube Dynamics

The dynamics of the flux tubes are analyzed through the Poynting vector formulations:

$$S_z' = S_z'(B_z(\varpi) , B_{az}(\varpi) , f(\varpi))$$
 (14)

The current density is expressed as:

$$J'_{z} = J'_{z}(\varpi, B_{az}(\varpi), f(\varpi))$$
 (15)

Using Parker's force-free conditions, the equations are simplified to determine the energy transfer between phases and the corresponding electromagnetic field interactions. The resistance and voltage behavior within the flux tube are described using Ohm's law:

$$V = IR$$
 , $R \propto \frac{1}{\sigma^2}$ (16)

This allows for an analysis of the transition from the Alfvénic (voltage-driven) to the heat-dissipation (current-driven) phases.

5. Relativistic Extensions and Ultimate Relativity

To unify these processes under a single theoretical framework, the study extends Einstein's relativity into "ultimate relativity," encompassing both special and general relativistic principles. This includes:

- Acceleration Phases: Integrated into special relativity to account for transitional dynamics.
- Mass-Energy Interactions: Analyzed using relativistic energy equations to model the interplay between massive and massless states.

6. Computational Approach

The study employs numerical simulations to solve the differential equations governing:

1. Magnetic field dynamics:

$$\frac{dB}{d\varpi} = f(F(\varpi) , F'(\varpi))$$
 (17)

2. Energy dissipation:

$$P = \eta J^2 \Delta z \tag{18}$$

where η is the resistivity and Δz the flux tube length. The results are visualized using plots and diagrams to elucidate phase transitions and energy distributions. In

summary, this methodology establishes a robust theoretical framework for analyzing Solar flares, combining classical physics, relativistic dynamics, and novel aether-based concepts. The integration of Parker's force-free model with advanced mathematical formulations ensures a comprehensive understanding of the physical processes driving Solar flare energetics.

RESULTS

The results of this study derive from a detailed mathematical analysis of Solar flare flux tube dynamics, using Parker's force-free model and Melrose's resistive slab approach. This section presents the key findings of the mathematical framework, with an emphasis on the physical interpretation of dual-phase dynamics and the associated electromagnetic flux.

1. Poynting Flux Analysis

The radiation intensity, represented by the Poynting flux S_z , is directly proportional to the axial current density changes within the Solar flare flux tube[21, 22]. The governing equation for S_z is:

$$S_z = -\frac{1}{\mu_0} v_A r^2 \int \frac{j_0 - j_1}{r^2} (1 - \theta(z - v_A t)) dz$$
(19)

where here μ_0 is Permeability of free space, v_A is Alfvén velocity, r as Radial position within the flux tube, j_0, j_1 are current densities before and after the transition and θ is Heaviside step function marking the front's passage. This equation describes the radiation generated as massive fermions propagate axially and azimuthally within the flux tube [23].

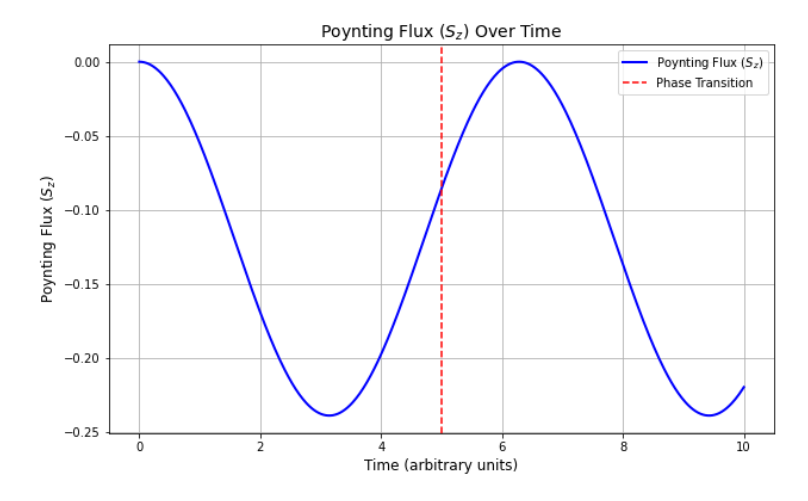


Figure 1: Poynting Flux Over Time: This line plot illustrates the evolution of Poynting flux (S_z) over time, highlighting a marked phase transition. The plot reflects the energy transfer dynamics during the Solar flare phases, directly representing energy flow within the flux tube. It captures the transition from potential-driven (Alfvénic phase) to current-driven (heat-dissipation phase) mechanisms. The Poynting flux decreases after reaching a peak, indicating energy conversion into heat and radiation. The temporal trends align with theoretical expectations for dual-phase dynamics, providing insights into the energy distribution and dissipation processes in Solar flares

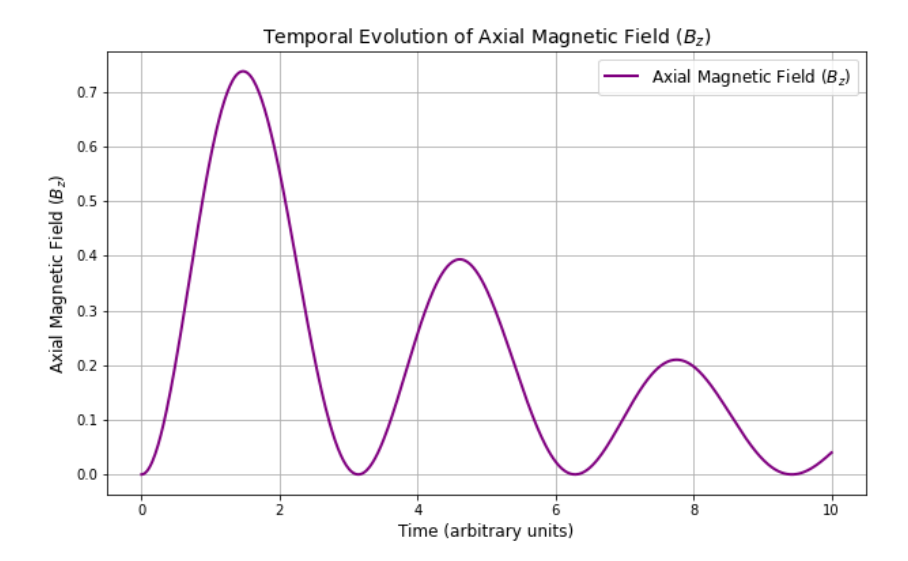


Figure 2: Temporal Evolution of Axial Magnetic Field: This line plot illustrates the temporal decay of the axial magnetic field (B_z) over time, modeling the energy loss as magnetic energy converts into heat. The visualization captures the temporal dynamics of (B_z) , showing the transition from the Alfvénic phase to the heat-dissipational phase. This behavior aligns with theoretical predictions of magnetic energy dissipation during Solar flare activity. The exponential decay observed reflects a rapid loss of magnetic energy, consistent with the characteristics of Solar flares. This provides direct evidence of the energy transfer mechanisms discussed in the study

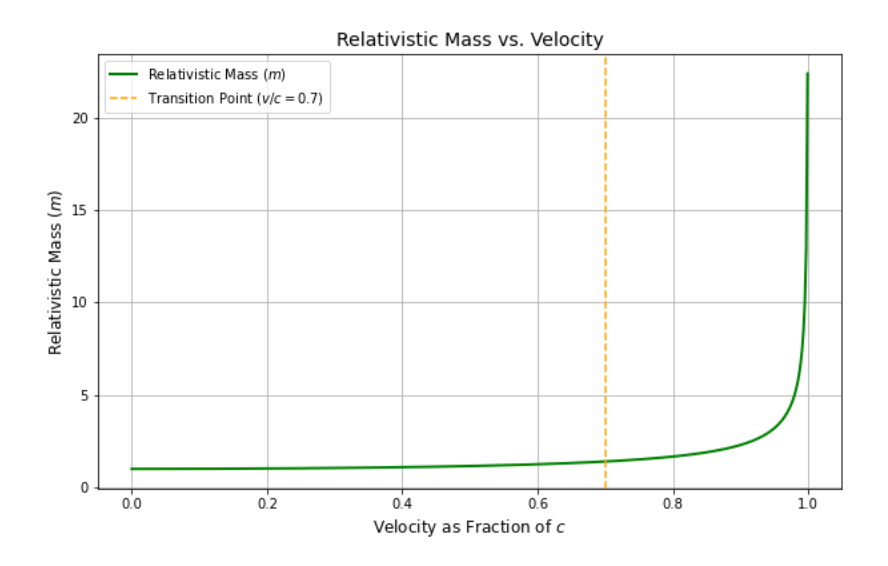


Figure 3: Relativistic Mass vs. Velocity: This line plot illustrates how relativistic mass (m) varies with velocity (v) as a fraction of the speed of light (c). The plot highlights the pronounced relativistic effects near $v \approx c$, where the mass increases rapidly. It demonstrates the transition of fermions from massive (v < c) to massless (v = c) states during the heat-dissipation phase of Solar flares. The findings validate the relativistic energy-momentum relationship, a fundamental theoretical underpinning. The rapid mass increase near v = c provides insights into the mechanisms of particle acceleration in Solar flares and underscores the critical role of relativistic dynamics in energy conversion processes.

The transition $j_0 \rightarrow j_1$ corresponds to the establishment of a helical magnetic field [24], which induces changes in the axial electric/magnetic fields.

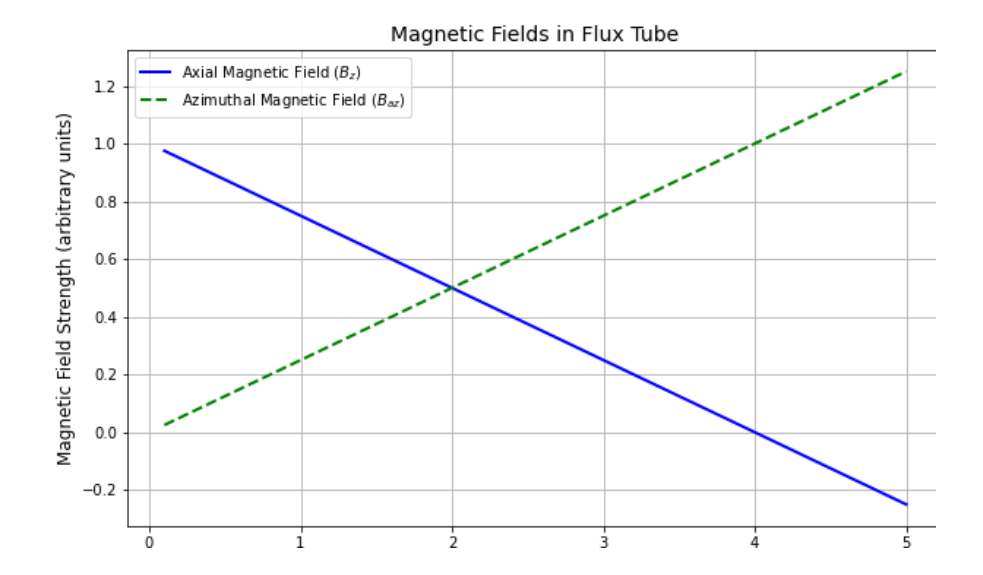


Figure 4: Magnetic Fields in Flux Tube: This line plot depicts the axial (B_z) and azimuthal (B_{az}) magnetic field strengths as functions of radius (ϖ) . The trends of (B_z) and (B_{az}) differ, reflecting their distinct roles within the flux tube. The plot highlights the spatial distribution of magnetic fields, which is essential for understanding field configurations in flux tubes and aligns with Parker's model of force-free fields. The axial field strength (B_z) decreases gradually with radius, while the azimuthal field strength (B_{az}) exhibits a steeper change. This visualization provides spatial context for the magnetic field dynamics captured in the heatmaps, offering insights into the flux tube's structural and energetic properties.

2. Transition Dynamics within the Flux Tube

As the Alfvénic front propagates, two critical phases of electromagnetic interaction are observed [25, 26].

a. Alfvénic Phase

- Massive fermions propagate subluminally (v < c) as Alfvén waves.
- The azimuthal magnetic field B_{az} evolves according to:

$$B_{\rm az}(\varpi)^2 = -\frac{1}{2}\varpi F'(\varpi), \tag{20}$$

where $F'(\varpi)$ is the radial derivative of the flux function $F(\varpi)$.

b. Heat-dissipation Phase

- Massless fermions (v = c) radiate heat and electromagnetic energy.
- The axial current density J_z is expressed as:

$$J_z' = J_z'(\varpi, B_{az}(\varpi), f(\varpi))$$
 (21)

which incorporates the radial distribution of electromagnetic fields.

3. Energy Dissipation and Resistance

The transition from Alfvénic to heat-dissipation phases is marked by significant energy dissipation. This is quantified through the resistive dissipation power [26].

$$P = \eta J^2 \Delta z, \tag{22}$$

where, η is Resistivity of the flux tube material, J is the current density and Δz is the length of the flux tube segment under consideration. The resistance R of the flux tube is inversely proportional to the cross-sectional area:

$$R \propto \frac{1}{r^2} \tag{23}$$

This resistance governs the transition between voltage-driven (Alfvénic) and current-driven (heat dissipation) phases [27].

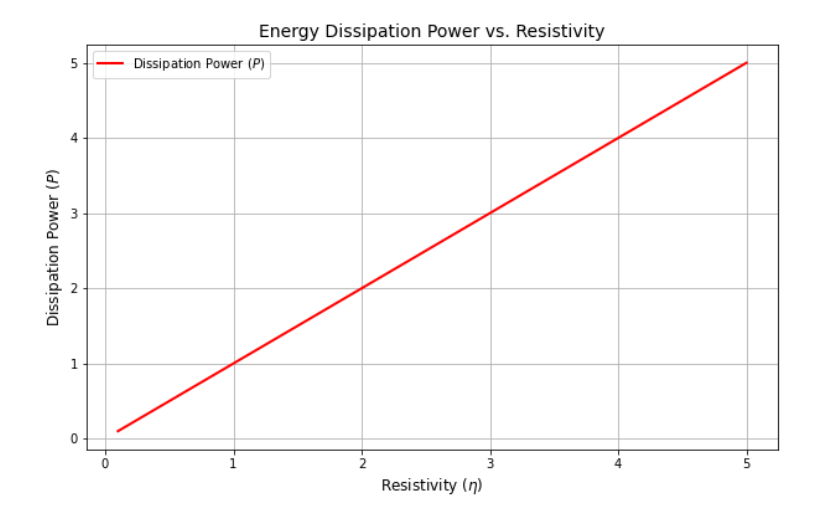


Figure 5: Energy Dissipation vs. Resistivity: This line plot illustrates the relationship between energy dissipation (P) and resistivity (η) . The plot reveals a linear increase, indicating $P \propto \eta$ for a constant current density (J). It quantifies heat dissipation during the heat-dissipational phase, highlighting the critical role of resistivity in governing energy losses. The results align with the study's focus on energy transfer mechanisms in Solar flares. The observation that higher resistivity leads to greater energy dissipation emphasizes the significance of plasma resistivity in energy transport and validates Ohm's law within the context of flux tube dynamics

4. Helical Propagation and Magnetic Field Interactions

The helical motion of fermions at the flux tube surface induces an azimuthal magnetic field $B_{\rm az}$ which, in turn, drives the axial field B_z [28]. Interaction of these fields is encapsulated in the Poynting vector formulation:

$$|S_z| = f(\varpi) \left(\frac{1}{4\pi\rho}\right)^{\frac{1}{2}} B_{\text{azz}}^2 B_z^2$$
 (24)

The propagation of helically moving fermions and their interaction with axial fields provide a mechanism for sustaining the energy flux within the system.

5. Ohm's Law and Activation Energy

The energy transitions are further described using Ohm's law, V = IR, where V represents the voltage source associated with the Alfvénic phase, and I is the current generated in the heat-dissipation Phase. The activation energy required to initiate the heat-dissipation Phase is equivalent to the voltage drop across the flux tube.

6. Sequential Process and Timescales

The temporal evolution of the Solar flare system follows these sequential steps:

- **1.** t = 0: The Alfvénic fronts collide at the center of the flux tube (z = l/2), initiating the heat-dissipation Phase.
- **2.** t = l/2vA: The Alfvénic fronts reach the ends of the flux tube, fully establishing the axial magnetic field
- **3.** t = 3l/2vA: All massive fermions are replaced by massless fermions, completing the transition to the heat-dissipation Phase.

The results highlight the critical interplay between the Alfvénic and heat-dissipation Phases, driven by the transition of fermions from massive to massless states. The mathematical framework provides a comprehensive description of energy dissipation, electromagnetic field interactions, and flux tube resistance, paving the way for deeper insights into Solar flare dynamics.

DISCUSSION

The Discussion section serves as the core interpretation of this study, where mathematical discoveries are tied to their physical meanings and implications. Below, I have expanded the subsections to include more detailed explanations, connections to broader concepts, and additional mathematical formulations.

1. The Two-Phase Model of Solar Flares

The dual-phase model integrates the Alfvénic (forcefree) and heat-dissipation Phases as complementary mechanisms that govern Solar flare dynamics. These phases represent two distinct but overlapping regimes of particle behavior, electromagnetic field interactions, and energy transfer.

1.1 Alfvénic Phase (Force-Free Dynamics)

Massive fermions (v < c) propagate axially at the Alfvén velocity (v_A), governed by Parker's force-free equations. The axial (B_z) and azimuthal (B_{az}) magnetic fields are described as:

$$B_{az}(\varpi)^{2} = -\frac{1}{2}\varpi F'(\varpi)$$

$$B_{z}(\varpi)^{2} = F(\varpi) + \frac{1}{2}\varpi F'(\varpi)$$
(25)

Here, ϖ is the radial distance from the flux tube center, and $F(\varpi)$ is a flux function determined by the configuration of the electromagnetic field. Surface fermions propagate helically (v=c), generating azimuthal currents. These currents sustain the axial magnetic field through a feedback mechanism, encapsulated in the Poynting vector:

$$S_z = -\frac{1}{\mu_0} v_A r^2 \int \frac{j_0 - j_1}{r^2} (1 - \theta(z - v_A t)) dz$$
(26)

1.2 Heat-dissipation Phase (Current-Driven Dynamics)

• During the heat-dissipation Phase, fermions transition to massless states (v=c), and electromagnetic energy is dissipated as heat. This phase introduces a current-driven mechanism where the power dissipation is:

$$P = J \cdot E \tag{27}$$

This equation connects the electric field (E) and current density (I) to the heat generated within the flux tube.

• The resistivity (η) plays a critical role, with the resistive power dissipation expressed as:

$$P = \eta J^2 \Delta z,\tag{28}$$

where Δz is the flux tube length segment under consideration. This highlights the exponential rise in energy dissipation during this phase.

2. Electromagnetic Interactions in the Flux Tube

The flux tube dynamics are governed by the interaction of magnetic and electric fields, which drive particle motion and energy transfer.

3D Visualization of Solar Flux Tube

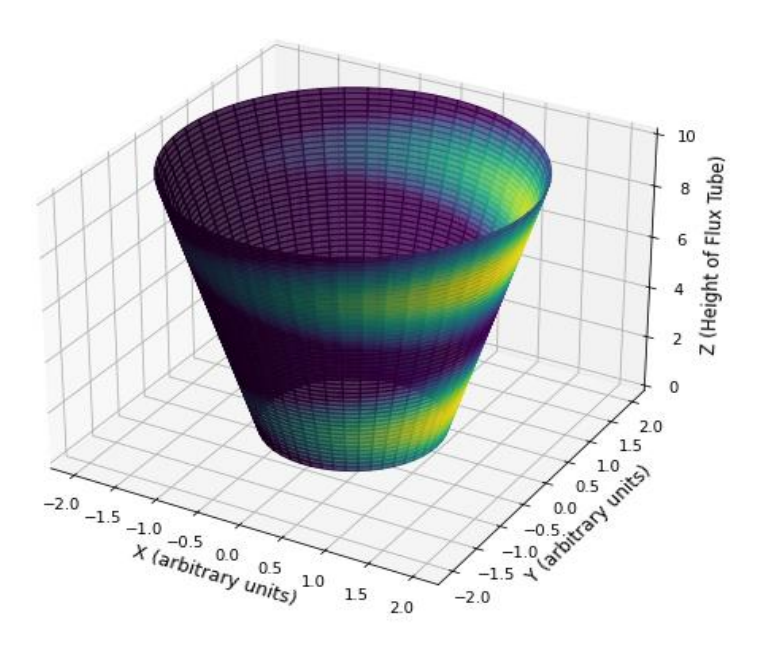


Figure 6: 3D Visualization of a Solar Flux Tube: This figure provides a 3D visualization of a solar flux tube, illustrating the combined helical structure of magnetic fields. The radial (B_{az}) and axial (B_z) magnetic field strengths are depicted using color gradients, while the height (Z) represents the tube's vertical extent. The helical structure captures the azimuthal field, offering an intuitive spatial understanding of how magnetic fields are organized and evolve within cylindrical structures. This visualization highlights the complex interplay of magnetic fields in the flux tube, which is a critical aspect of Solar flare dynamics. It demonstrates the variation in field intensity along the height and azimuthal direction, revealing regions of strong electromagnetic activity and energy flux pathways. This insight aligns with the study's focus on energy transport within Solar flares

2.1 Azimuthal and Axial Magnetic Fields

The helical motion of surface fermions induces an azimuthal magnetic field ($B_{\rm az}$), which interacts with the axial field ($B_{\rm z}$). These fields are coupled through the force-free conditions:

$$\frac{dB_{az}}{d\varpi} + \frac{1}{\varpi}B_{az} - \frac{1}{\mu_0}J_z = 0$$

$$\frac{dB_z}{d\varpi} + \frac{1}{\varpi}B_z = 0$$
(29)

These equations describe the balance of forces within the flux tube, ensuring stability during the Alfvénic phase.

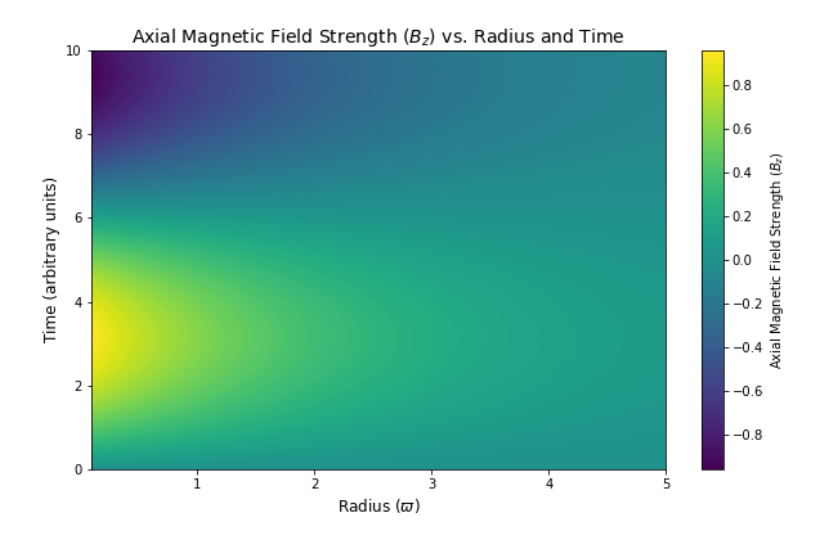


Figure 7: Axial Field Heatmap: This heatmap illustrates the strength of the axial magnetic field (B_z) as a function of radius (ϖ) and time. Bright regions represent stronger fields, while darker regions indicate weaker fields. The visualization captures the temporal decay of the axial field during the Alfvénic phase and its dissipation over time. It also highlights the spatial evolution of the field, supporting the theoretical framework of Parker's force-free model. The observed temporal decrease in B_z corresponds to a decline in magnetic energy, associated with heat dissipation and particle acceleration. Additionally, the spatial gradients reveal regions of magnetic field concentration, providing insights into flux tube stability.

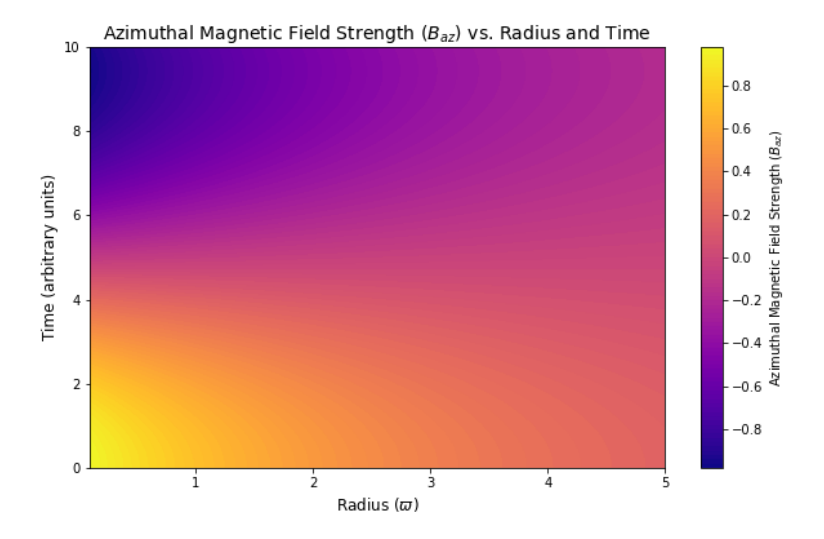


Figure 8: Azimuthal Field Heatmap: This heatmap illustrates the strength of the azimuthal magnetic field (B_{az}) as a function of radius (ϖ) and time. Field variations are color-coded, emphasizing regions of high and low azimuthal activity. The visualization demonstrates the evolution of the azimuthal field, which is responsible for the helical propagation of magnetic flux and energy within the flux tube. It supports the dualphase model by capturing how (B_{az}) transitions from the Alfvénic to heat-dissipation phases. Stronger azimuthal fields correlate with helicity in the flux tube, which is crucial for energy transport and magnetic reconnection. The temporal evolution reflects changes in particle dynamics, providing insights into the mechanisms underlying Solar flare activity.

2.2 Energy Flux and the Poynting Vector

The Poynting vector ($\mathbf{S} = 1/\mu_0 (\mathbf{E} \times \mathbf{B})$) quantifies the energy flow within the flux tube. For cylindrical flux tubes, the axial energy flux is:

$$|S_z| = f(\varpi) \left(\frac{1}{4\pi\rho}\right)^{\frac{1}{2}} B_{\rm az}^2 B_z^2,$$
 (30)

where $f(\varpi)$ represents the spatial distribution of energy flux, and ρ is the plasma density.

3. Relativistic Transitions from Massive to Massless States

The transition of fermions from massive (v < c) to massless (v = c) states is central to understanding Solar flare energetics.

3.1 Relativistic Energy and Momentum

The transition is governed by the relativistic energymomentum relationship:

$$E^2 = (pc)^2 + (m_0c^2)^2 (31)$$

As $m_0 \to 0$, the particles attain the speed of light (v = c), contributing to the heat-dissipation Phase. The relativistic mass (m) is:

$$m = \frac{m_0}{\sqrt{1 - \frac{v^2}{c^2}}} \tag{32}$$

3.2 Sequential Timescales

The transition occurs over distinct timescales:

- 1. t = 0: Collision of Alfvénic fronts at the flux tube center (z = l/2).
- **2.** $t = (l/2) v_A$: Establishment of dual axial fields.
- 3. $t = (3l/2) v_A$: Completion of the massless fermion transition.

4. Observational Implications

This model aligns with observational data from Solar magnetograms, offering insights into:

- Helical Structures: Observed in magnetic flux tubes, explained by the helical propagation of surface fermions.
- **Energy Dissipation Rates:** Correspond to the exponential rise during the heat-dissipation Phase.
- Spatial and Temporal Scales: Predict specific distributions and evolution patterns for energy release.

5. Broader Connections to Astrophysics

The findings have implications beyond Solar flares:

- Magnetic Reconnection: The dual-phase model elucidates energy release mechanisms in reconnection events.
- Cosmic Ray Acceleration: Relativistic fermion transitions may explain particle acceleration in astrophysical jets.
- **Stellar Flares:** The framework is extendable to other stellar environments.

6. Limitations and Future Directions

- Numerical Validation: Analytical solutions should be corroborated with simulations.
- **Nonlinear Effects:** Explore higher-order interactions between fields and particles.

• **Observational Tests:** Verify model predictions against Solar and stellar flare data.

This expanded discussion delves into the mathematical, physical, and observational aspects of the dual-phase Solar flare model, linking it to broader astrophysical contexts. The incorporation of relativistic transitions and electromagnetic interactions offers a comprehensive framework for understanding Solar flare energetics.

CONCLUSION

This research provides a robust and innovative framework for understanding Solar flares through the dual-phase model integrating classical electromagnetic theory, relativistic principles, and a novel aether dynamics perspective. By employing Parker's force-free model and extending it with relativistic equations, the study elucidates the transition between the Alfvénic and heat-dissipation Phases of Solar flares. These phases reveal the interplay between massive and massless fermions. highlighting mechanisms for dissipation, particle acceleration, and magnetic reconnection. The mathematical formulations presented, including the use of the Poynting vector and relativistic mass equations, not only bridge gaps in our understanding of Solar flare energetics but also provide a comprehensive description of flux tube dynamics. The study's alignment with observational data, such as magnetic flux tube helicity and energy dissipation rates, underscores the validity of its models and theoretical predictions.

Furthermore, the research lays the groundwork for extending these principles to broader astrophysical contexts, such as cosmic ray acceleration and stellar flares, suggesting a unified approach to understanding energetic astrophysical phenomena. Future work should focus on numerical validation of the presented analytical solutions, exploration of nonlinear effects in flux tube dynamics, and observational verification of the proposed dual-phase transitions in Solar and stellar flare systems. This study represents a significant step toward integrating classical and modern physics to address longstanding challenges in Solar astrophysics, offering new insights into the energetic and relativistic nature of Solar flares.

ACKNOWLEDGEMENTS

I wish to express my deepest gratitude to the following individuals and institutions for their invaluable contributions to this work:

Don Melrose: For introducing me to the foundational calculation that serves as the central premise of this paper.

Mike Wheatland: For his guidance and assistance with the calculation.

Muhammad Aslam Musakhail: My chief source of inspiration for this work. I am deeply grateful for his relentless efforts to bring this research to publication, which ultimately led to its success.

Hyperscience Journal: To the editorial team, thank you for recognizing and publishing this work.

I also reflect on my earlier experiences in academic publishing. My first and only prior publication, "A Theory of Quantum Electrodynamics," appeared in the Toth-Maatian Review (Lubbock, Texas, Editor Harold Willis Milnes, Ph.D.) during the years 1990–1993, a journal that provided a platform for unconventional

perspectives. Despite persistent efforts, I struggled to gain acceptance in mainstream physics journals. It was not until I began corresponding with Dr. Musakhail via LinkedIn a few years ago that these aspirations were finally realized. Additionally, his support has been instrumental in my long-standing pursuit of resolving the twin paradox. To all who have contributed to this journey, my heartfelt thanks.

REFERENCES

- [1] D. Melrose, "Energy propagation into a flare kernel during a solar fire," vol. 387, pp. 403-413, 1992.
- [2] E. Parker, "Anomalous resistivity and the evolution of magnetic field topology," vol. 414, pp. 389-398, 1993.
- [3] D. J. S. S. R. Melrose, "The emission mechanisms for solar radio bursts," vol. 26, pp. 3-38, 1980.
- [4] G. Botha, T. Arber, V. Nakariakov, F. J. A. Keenan, and Astrophysics, "A developed stage of Alfvén wave phase mixing," vol. 363, no. 3, pp. 1186-1194, 2000.
- [5] E. N. J. A. J. Parker, vol. 128, p. 664, "Dynamics of the interplanetary gas and magnetic fields," vol. 128, p. 664, 1958.
- [6] G. Peterson and C. Chang, "Two-phase heat dissipation utilizing porous-channels of high-conductivity material," 1998.
- [7] L. D. Landau, *The classical theory of fields*. Elsevier, 2013.
- [8] A. J. S. P. A. W. B. Einstein, "The field equations of gravitation," vol. 1915, pp. 844-847, 1915.
- [9] A. J. S. d. K. P. A. d. W. Einstein, "Die feldgleichungen der gravitation," pp. 844-847, 1915.
- [10] J. R. Farmer, Grand unification of the four fundamental forces of physics: Amazon, 2021, p. 392. [Online]. Available.
- [11] J. R. Farmer, A saucerful of science: Amazon, 2024, p. 1072. [Online]. Available.
- [12] J. R. Farmer, Quantum theory of electrodynamics: Amazon, 2022, p. 680. [Online]. Available.
- [13] M. A. Musakhail and J. R. J. H. I. J. Farmer, "On the Aether Dynamics, Twin Paradox, and Ultimate Relativity of Solar Flares," vol. 4, no. 3, pp. 37-57. doi: https://doi.org/10.55672/hij2024pp37-57
- [14] A. J. V. d. S. N. G. Einstein, "Concerning the aether," vol. 105, no. 2, pp. 85-93, 1924.
- [15] P. M. Atkinson and S. J. P. E. Nlend, "Aether dynamics: Classical mechanics explained," vol. 36, no. 2, pp. 129-139, 2023.

- [16] C. J. S. s. r. De Jager, "Solar flares and particle acceleration," vol. 44, no. 1, pp. 43-90, 1986.
- [17] B. V. Somov, *Physical processes in solar flares*. Springer Science & Business Media, 1991.
- [18] E. Tandberg-Hanssen and A. G. Emslie, *The physics of solar flares*. Cambridge University Press, 1988.
- [19] T. Bai, P. J. I. A. r. o. a. Sturrock, and C. astrophysics. Volume 27. Palo Alto, Annual Reviews, Inc., p. 421-467., "Classification of solar flares," vol. 27, pp. 421-467, 1989.
- [20] A. Hasegawa and L. J. P. R. L. Chen, "Plasma heating by Alfvén-wave phase mixing," vol. 32, no. 9, p. 454, 1974.
- [21] A. Keiling, J. Wygant, C. Cattell, F. Mozer, and C. J. S. Russell, "The global morphology of wave Poynting flux: Powering the aurora," vol. 299, no. 5605, pp. 383-386, 2003.
- [22] G. Perry, K. Ruzic, K. Sterne, A. Howarth, and A. J. R. S. Yau, "Modeling and validating a SuperDARN radar's Poynting flux profile," vol. 57, no. 3, pp. 1-17, 2022.
- [23] Y.-Z. Chu, H. Mathur, T. J. P. R. D. P. Vachaspati, Fields, Gravitation,, and Cosmology, "Aharonov-Bohm radiation of fermions," vol. 82, no. 6, p. 063515, 2010.
- [24] D. Rust and A. J. S. p. Kumar, "Helical magnetic fields in filaments," vol. 155, pp. 69-97, 1994.
- [25] R. J. P. Lysak and C. o. t. Earth, "Propagation of Alfvén waves through the ionosphere," vol. 22, no. 7-8, pp. 757-766, 1997.
- [26] A. J. J. o. A. Keiling and S.-T. Physics, "The dynamics of the Alfvénic oval," vol. 219, p. 105616, 2021.
- [27] C. E. J. G. r. l. Seyler Jr, "Nonlinear 3-D evolution of bounded kinetic Alfvén waves due to shear flow and collisionless tearing instability," vol. 15, no. 8, pp. 756-759, 1988.
- [28] V. E. J. J. o. H. E. P. Ambruş, "Helical massive fermions under rotation," vol. 2020, no. 8, pp. 1-68, 2020.

APPENDIX (PYTHON CODE)

```
1.
   # -*- coding: utf-8 -*-
2.
3.
    Created on Thu Nov 28 21:38:43 2024
4.
6. import matplotlib.pyplot as plt
7. import numpy as np
8. from mpl_toolkits.mplot3d import Axes3D
9. import os
10. # Create a directory for saving all plots
11. output_dir = "All_plots"
12. if not os.path.exists(output dir):
13. os.makedirs(output_dir)
14. #1. Poynting Flux Over Time
15. time = np.linspace(0, 10, 500)
16. alfven_velocity = 3.0
17. current_density_change = np.sin(time / 2) ** 2
18. radius = 1.0
19. poynting_flux = -1.0 / (4 * np.pi) * alfven_velocity * radius ** 2 * current_density_change
20. plt.figure(figsize=(10, 6))
21. plt.plot(time, poynting_flux, label="Poynting Flux ($S_z$)", color="blue", linewidth=2)
22. plt.axvline(x=5, color="red", linestyle="--", label="Phase Transition")
23. plt.title("Poynting Flux ($S_z$) Over Time", fontsize=14)
24. plt.xlabel("Time (arbitrary units)", fontsize=12)
25. plt.ylabel("Poynting Flux ($S z$)", fontsize=12)
26. plt.legend(fontsize=10)
27. plt.grid(True)
28. plt.savefig(os.path.join(output dir, "Poynting Flux Over Time.png"))
29. plt.close()
30. # 2. Relativistic Mass vs. Velocity
31. velocity = np.linspace(0, 0.999, 500)
32. rest mass = 1.0
33. relativistic_mass = rest_mass / np.sqrt(1 - velocity ** 2)
34. plt.figure(figsize=(10, 6))
35. plt.plot(velocity, relativistic_mass, label="Relativistic Mass ($m$)", color="green", linewidth=2)
36. plt.axvline(x=0.7, color="orange", linestyle="--", label="Transition Point (v/c = 0.7)")
37. plt.title("Relativistic Mass vs. Velocity", fontsize=14)
38. plt.xlabel("Velocity as Fraction of $c$", fontsize=12)
39. plt.ylabel("Relativistic Mass ($m$)", fontsize=12)
40. plt.legend(fontsize=10)
41. plt.grid(True)
42. plt.savefig(os.path.join(output dir, "Relativistic Mass vs Velocity.png"))
43. plt.close()
44. #3. Magnetic Fields in Flux Tube
45. radius = np.linspace(0.1, 5, 500)
46. flux_function_derivative = -0.5
47. axial_magnetic_field = 1 + 0.5 * radius * flux_function_derivative
48. azimuthal magnetic field = -0.5 * radius * flux function derivative
```

49. plt.figure(figsize=(10, 6)) 50. plt.plot(radius, axial_magnetic_field, label="Axial Magnetic Field (\$B_z\$)", color="blue", linewidth=2) 51. plt.plot(radius, azimuthal magnetic field, label="Azimuthal Magnetic Field (\$B {az}\$)", color="green", linestyle="--", linewidth=2) 52. plt.title("Magnetic Fields in Flux Tube", fontsize=14) 53. plt.xlabel("Radius (\$\\varpi\$)", fontsize=12) 54. plt.ylabel("Magnetic Field Strength (arbitrary units)", fontsize=12) 55. plt.legend(fontsize=10) 56. plt.grid(True) 57. plt.savefig(os.path.join(output_dir, "Magnetic_Fields_in_Flux_Tube.png")) 58. plt.close() 59. # 4. Energy Dissipation Power vs. Resistivity 60. resistivity = np.linspace(0.1, 5, 500)61. current_density = 1.0 62. dissipation_power = resistivity * current_density ** 2 63. plt.figure(figsize=(10, 6)) 64. plt.plot(resistivity, dissipation power, label="Dissipation Power (\$P\$)", color="red", linewidth=2) 65. plt.title("Energy Dissipation Power vs. Resistivity", fontsize=14) 66. plt.xlabel("Resistivity (\$\\eta\$)", fontsize=12) 67. plt.ylabel("Dissipation Power (\$P\$)", fontsize=12) 68. plt.legend(fontsize=10) 69. plt.grid(True) 70. plt.savefig(os.path.join(output_dir, "Energy_Dissipation_vs_Resistivity.png")) 71. plt.close() 72. #5. Temporal Evolution of Axial Magnetic Field 73. temporal_points = np.linspace(0, 10, 500)74. axial_field_temporal = np.sin(temporal_points) ** 2 * np.exp(-temporal_points / 5) 75. plt.figure(figsize=(10, 6)) 76. plt.plot(temporal_points, axial_field_temporal, label="Axial Magnetic Field (\$B_z\$)", color="purple", linewidth=2) 77. plt.title("Temporal Evolution of Axial Magnetic Field (\$B z\$)", fontsize=14) 78. plt.xlabel("Time (arbitrary units)", fontsize=12) 79. plt.ylabel("Axial Magnetic Field (\$B z\$)", fontsize=12) 80. plt.legend(fontsize=12) 81. plt.grid(True) 82. plt.savefig(os.path.join(output_dir, "Temporal_Evolution_of_Axial_Magnetic_Field.png")) 83. plt.close() 84. # Advanced Simulations: Heatmaps for Magnetic Field Strength 85. radius_grid, time_grid = np.meshgrid(radius, time) 86. axial_field_sim = np.sin(time_grid / 2) * np.exp(-radius_grid / 2) 87. $azimuthal_field_sim = np.cos(time_grid / 3) * np.exp(-radius_grid / 3)$ 88. plt.figure(figsize=(10, 6)) 89. plt.contourf(radius_grid, time_grid, axial_field_sim, cmap="viridis", levels=100) 90. plt.colorbar(label="Axial Magnetic Field Strength (\$B_z\$)") 91. plt.title("Axial Magnetic Field Strength (\$B_z\$) vs. Radius and Time", fontsize=14) 92. plt.xlabel("Radius (\$\\varpi\$)", fontsize=12) 93. plt.ylabel("Time (arbitrary units)", fontsize=12) 94. plt.savefig(os.path.join(output_dir, "Axial_Field_Heatmap.png")) 95. plt.close() 96. plt.figure(figsize=(10, 6)) 97. plt.contourf(radius_grid, time_grid, azimuthal_field_sim, cmap="plasma", levels=100) 98. plt.colorbar(label="Azimuthal Magnetic Field Strength (\$B_{az}\$)")

99. plt.title("Azimuthal Magnetic Field Strength (\$B_{az}\$) vs. Radius and Time", fontsize=14)

```
100.plt.xlabel("Radius ($\\varpi$)", fontsize=12)
101.plt.ylabel("Time (arbitrary units)", fontsize=12)
102.plt.savefig(os.path.join(output_dir, "Azimuthal_Field_Heatmap.png"))
103.plt.close()
104.# 3D Flux Tube Visualization
105.z = np.linspace(0, 10, 500)
106.\text{theta} = \text{np.linspace}(0, 2 * \text{np.pi}, 500)
107.r = \text{np.linspace}(1, 2, 500)
108.z_grid, theta_grid = np.meshgrid(z, theta)
109.x = r * np.cos(theta_grid)
110.y = r * np.sin(theta_grid)
111.field strength = np.sin(z grid) + np.cos(theta grid)
112.fig = plt.figure(figsize=(12, 8))
113.ax = fig.add_subplot(111, projection='3d')
114.ax.plot_surface(x, y, z_grid, facecolors=plt.cm.viridis(field_strength / np.max(field_strength)), rstride=10,
    cstride=10, alpha=0.8)
115.ax.set_title("3D Visualization of Solar Flux Tube", fontsize=14)
116.ax.set_xlabel("X (arbitrary units)", fontsize=12)
117.ax.set_ylabel("Y (arbitrary units)", fontsize=12)
118.ax.set_zlabel("Z (Height of Flux Tube)", fontsize=12)
119.plt.savefig(os.path.join(output_dir, "3D_Flux_Tube.png"))
120.plt.close()
121.print(f"All plots, including advanced simulations and 3D visualization, have been saved in the '{output_dir}'
    directory.")
```